Tuijin Jishu/Journal of Propulsion Technology
ISSN: 1001-4055
Vol. 45 No. 3 (2024)

# Characteristics of Radiating Carreau-Nanofluid Flow Past a Permeable Stretching Sheet with the Effects of Magnetic Field and Transpiration

**[1]D.R.Kirubaharan, [2]A.D Subhashini, [3]G.Murali[*]**
*[1,2]Department of Mathematics, PRIST University,Thanjavur, India.*
*[3]Department of Mathematics, Geethanjali College of Engineering and technology,Cheeryal,India.*

***Abstract:*** The steady-state flow across an isothermal, permeable stretched sheet of an incompressible, viscous, and electrically conducting Carreau fluid is investigated in this work. It considers Brownian motion, a magnetic field, transpiration, thermophoresis, concentration and thermal slip, and thermal radiation. Buongiorno's model manages the Brownian motion and thermophoresis in the regulating equations for energy and concentration. Local similarity transformations let one convert the governing partial differential equations into a collection of ordinary differential equations. These nonlinear ordinary differential equations then numerically are solved in concert with the RK-method utilizing a strong numerical approach known as shooting technique. The study investigates how various physical properties influence the graphical depictions of profiles of temperature, speed, and concentration of nanoparticles. In several situations the findings show excellent consistency with earlier investigations.

***Keywords:*** Transpiration effect; Magnetic field; Carreau fluid; Nanofluid; Thermal radiation; Permeable Stretching sheet;RK-method; Shooting technique

## 1. Introduction

Carreau fluids are an intriguing subject for the study of fluid dynamics because of their non-Newtonian properties, especially when combined with nanofluid particles. Nanofluids are formed by the incorporation of nanoparticles into regular fluids, resulting in improved properties and efficiency. This combination has the ability to greatly improve heat transmission, rheological qualities, and other crucial aspects that are essential for several technological applications. This session will explore the intricate behavior of Carreau fluids when they are mixed with nanofluid particles. This research will examine the influence of this combination on several domains, including industrial processes and biological applications. In order to address the limitations of the power law model in accurately calculating viscosity at very high and low shear rates, Carreau [1] developed the Carreau model. Salahuddin and his colleagues [2] investigated the motion of a Carreau-Yasuda fluid with magnetohydrodynamics (MHD) characteristics across a compressed sensor surface. Sulochana [3] examined the influence of transpiration on the movement of Carreau nanofluid under the effects of magnetohydrodynamics at a stagnation point on a stretched surface. Khan et al. [4] examined the thermal and mass transfer characteristics of a Carreau nanofluid on a computationally expanding or contracting cylinder. Khan and Azam [5] examined the dynamic characteristics of heat and mass transmission in a Carreau nanofluid over a stretched surface, while also considering the influence of magnetohydrodynamics. Khan and his colleagues [6] performed a computational analysis on the turbulent Falkner-Skan flow in Carreau nanofluid. The researchers examined the effects of the magnetic field and the convective boundary condition. Raju and Sandeep [7] examined the transfer of mass and heat in the Falkner-Skan flow of Carreau fluid across a wedge, taking into consideration the effects of cross diffusion and a magnetic field. Khan et al. [8] investigated the flow characteristics of 2D Carreau-Yasuda flow across a heated surface, taking into consideration the impacts of Dufour and Soret's effects. Waqas and his colleagues [9] conducted an analysis on a set of partial differential equations (PDEs) that explain the

behavior of a Carreau-Yasuda fluid as it flows over an expanding surface. The equations also included partial slip, chemical reaction, heat radiation, and bio-convection. Riaz et al. [10] examined the motion of a Carreau nanofluid in a microchannel, taking into account its three-dimensional structure and temporal variations. Hayat et al. [11] investigated the movement of Carreau fluid over a stretched permeable sheet in a two-dimensional barrier layer. Waqas and his coauthors did a research on the unique characteristics of a magneto-hydrodynamic Carreau nanofluid [12]. The researchers analyzed the behavior of this nanofluid under different situations. The researchers conducted an analysis on the mobility of an MHD Carreau nanofluid system in both two and three dimensions, in addition to studying a chemical reaction. This work is referenced in the following citations: [13], [14], [15], [16], [17], [18], [19], [20], [21], [22], and [23]. The works mentioned in the literature [26–34] had a significant impact on understanding the nature of the reported work.

The aim of this study is to calculate the numerical solutions for the movement of a two-dimensional, viscous, electrically conducting, non-Newtonian Carreau fluid towards a permeable stretched sheet with a constant temperature. The calculations will be based on the previously stated references. This study examines the impacts of heat radiation, Brownian motion, magnetic field, thermophoresis, and nanofluid particles. The controlling partial differential equations are transformed into a set of nonlinear ordinary differential equations by the use of local similarity transformations. Afterwards, the equations are numerically solved using the RK-method and shot technique to analyze the influence of various physical factors on flow variables, including temperature, concentration, and velocity, using graphical analysis. Ultimately, a thorough examination is conducted to confirm the accuracy of the current study by comparing it to the existing body of research.

## 2. Flow Governing Equations

This research investigates the impact of heat radiation and a magnetic field on the flow of a non-Newtonian Carreau-nanofluid. The flow is constant, incompressible, viscous, and electrically conducting. It occurs towards a stretched sheet that is permeable but not linearly isothermal. The study also considers the existence of a transpiration effect. Figure 1 illustrates the physical coordinate system of this flow at $y = 0$. The investigation is based on the following assumptions:

i. Flow generation is caused by non-linear stretching of the sheet when two equal and opposing pressures are applied simultaneously along the $x$-axis.

ii. The sheet is extended with a velocity $u_w = ax^n$ with the origin location fixed, where the power-law index, $n$ is a non-linear stretching parameter, $a$ is a constant and $x$ is the coordinate orientated parallel to the stretching surface.

*Stretching Carreau-nanofluid sheet momentum, thermal and species boundary layers*

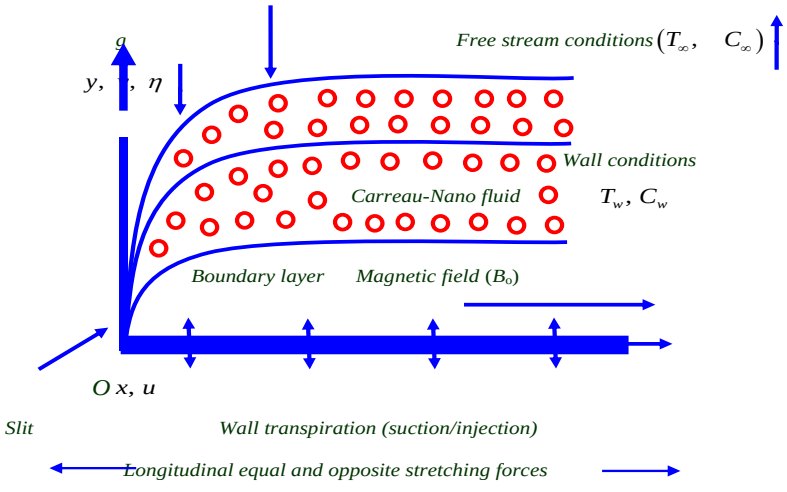


**Fig. 1. Geometry representation of the fluid**

iii. It is assumed as, the plate with constant surface temperature $T_w$ and concentration $C_w$ is placed in a gentle fluid of constant ambient temperature $T_\infty$ and concentration $C_\infty$.

iv. Normally, a variable magnetic field *B*(*x*) will be provided to the surface of the sheet while the magnetic field induced is minimal and may be justified for MHD flow at the small magnetic Reynolds number.

The conservation equations for mass, momentum, energy, and nano-particle species, ignoring buoyancy forces, edge effects, and the existence of a pressure gradient, are as follows:

*Continuity Equation:*

$$\frac{\partial u}{\partial x}+\frac{\partial v}{\partial y}=0 \quad (1)$$

*Momentum Equation:*

$$u\left(\frac{\partial u}{\partial x}\right)+v\left(\frac{\partial u}{\partial y}\right)=\nu\left\{1+\left[\frac{3(n-1)}{2}\right]\lambda^2\left(\frac{\partial u}{\partial y}\right)^2\right\}\left(\frac{\partial^2 u}{\partial y^2}\right)-\left(\frac{\sigma B_o^2}{\rho}\right)u-\left(\frac{\nu}{K_o}\right)u \quad (2)$$

*Equation of thermal energy:*

$$u\frac{\partial T}{\partial x}+v\frac{\partial T}{\partial y}=\alpha_m\nabla^2 T+\tau\left\{D_B\frac{\partial C}{\partial y}\frac{\partial T}{\partial y}+\frac{D_T}{T_\infty}\left(\frac{\partial T}{\partial y}\right)^2\right\}-\frac{1}{\rho C_p}\left(\frac{\partial q_r}{\partial y}\right) \quad (3)$$

The radiative heat flux $q_r$ (using Roselandapproximation) is defined as

$$q_r=-\frac{4\sigma^*}{3K^*}\left(\frac{\partial T^4}{\partial y}\right)$$

(4)

We assume that the temperature variances inside the flow are such that the term $T^4$ can be represented as linear function of temperature. This is accomplished by expanding $T^4$ in a Taylor series about a free stream temperature $T_\infty$ as follows:

$$T^4=T_\infty^4+4T_\infty^3(T-T_\infty)+6T_\infty^2(T-T_\infty)^2+\ldots\ldots\ldots$$

(5)

After neglecting higher-order terms in the above equation beyond the first-degree term in $(T-T_\infty)$, we get

$$T^4\cong 4T_\infty^3T-3T_\infty^4$$

(6)

Thus substituting Eq. (8) in Eq. (7), weget

$$q_r=-\frac{16T_\infty^3\sigma^*}{3K^*}\left(\frac{\partial T}{\partial y}\right) \quad (7)$$

Using (9), Eq. (5) can be written as

$$u\frac{\partial T}{\partial x}+v\frac{\partial T}{\partial y}=\alpha_m\nabla^2 T+\tau\left\{D_B\frac{\partial C}{\partial y}\frac{\partial T}{\partial y}+\frac{D_T}{T_\infty}\left(\frac{\partial T}{\partial y}\right)^2\right\}+\frac{1}{\rho C_p}\left(\frac{16T_\infty^3\sigma^*}{3K^*}\right)\left(\frac{\partial^2 T}{\partial y^2}\right) \quad (8)$$

*Equation of species concentration:*

$$u\frac{\partial C}{\partial x}+v\frac{\partial C}{\partial y}=D_B\frac{\partial^2 C}{\partial y^2}+\frac{D_T}{T_\infty}\frac{\partial^2 T}{\partial y^2} \tag{9}$$

The boundary conditions for Carreau-nano fluid flow are

$$\left.\begin{aligned} &u=u_w(x)=ax^n,\ v=v_w(x),\ T=T_w,\ C=C_w\ \ at\ \ y=0\\ &u\to 0,\ v\to 0,\ \ T\to T_\infty,\ C\to C_\infty\ \ as\ \ y\to\infty \end{aligned}\right\} \tag{10}$$

Where $v_w(x)$ is the variable velocity components in vertical direction at the stretching surface in which $v_w(x)$ < 0 represents to the suction cases and $v_w(x)$ >0 represent to the injection ones. The wall transverse velocity condition in (12) differs from that in Rana and Bhargava [24] since *wall transpiration* is now included. The following similarity variables are introduced for solving governing equations (4), (5) and (10) as

$$\left.\begin{aligned} &\eta=y\sqrt{\frac{a(n+1)}{2\nu}}x^{\frac{n-1}{2}},\ v=-\sqrt{\frac{a\nu(n+1)}{2}}x^{\frac{n-1}{2}}\left[f(\eta)+\left(\frac{n-1}{n+1}\right)\eta f'(\eta)\right],\\ &\theta(\eta)=\frac{T-T_\infty}{T_w-T_\infty},\ \phi(\eta)=\frac{C-C_\infty}{C_w-C_\infty},\ u=ax^n f'(\eta) \end{aligned}\right\} \tag{11}$$

Using Eq. (11), the fundamental Eqs. (2), (3) to (8) become

$$f'''+ff''-\left(\frac{2n}{n+1}\right)f'^2-Mf'+\frac{3(n-1)}{2}Wef''^2ff'''-Kf'=0 \tag{12}$$

$$\left(1+\frac{4R}{3}\right)\theta''+\Pr f\theta'+\Pr Nb\theta'\phi'+\Pr Nt\theta'^2=0 \tag{13}$$

$$2Nb\phi''+NbLef\phi'+2Nt\theta''=0 \tag{14}$$

and the corresponding boundary conditions (10) become

$$\left.\begin{aligned} &f=f_w,\ f'=1,\ \theta=1,\ \phi=1\ \ \ at\ \ \ \eta=0\\ &f'\to 0,\ \theta\to 0,\ \ \phi\to 0\ \ \ as\ \ \ \eta\to\infty \end{aligned}\right\} \tag{15}$$

where the involved physical parameters are defined as

$$\left.\begin{aligned} &\Pr=\frac{\nu}{\alpha},\ M=\frac{\sigma B_o^2 x}{\rho a},\ Nb=\frac{(\rho C)_p D_B(C_w-C_\infty)}{(\rho C)_f\nu},\ R=\frac{4\sigma^* T_\infty^3}{\kappa K^*},\ Le=\frac{\nu}{D_B},\\ &Nt=\frac{(\rho C)_p D_T(T_w-T_\infty)}{(\rho C)_f\nu T_\infty},\ f_w=-\frac{v_w(x)}{\sqrt{\frac{a\nu(n+1)}{2}}x^{\frac{n-1}{2}}},\ We=\frac{a^2x^2\lambda^2}{\nu},\ K=\frac{\nu}{aK_o}, \end{aligned}\right\}$$

(16)

The parameters of engineering interest in heat and mass transport problems are the Skin-friction coefficient $(Cf)$, local Nusselt number $(Nu_x)$ and the Sherwood number $(Sh_x)$. These parameters characterise the skin-friction coefficient, wall heat, mass transfer rates, respectively, and are defined by

$$Cf=\frac{\tau_w}{\rho a^2}\ \text{where}\ \tau_w=\frac{\partial u}{\partial x}+\frac{(n-1)}{2}\lambda^2\left(\frac{\partial u}{\partial y}\right)^3\Rightarrow Cf=\frac{1}{\sqrt{\mathrm{Re}_x}}\left\{f''(0)+\frac{(n-1)}{2}We\left[f''(0)\right]^3\right\} \tag{17}$$

$$Nu_x = \frac{xq_w}{\kappa\left(T_w - T_\infty\right)} \text{ Where } q_w = -\kappa\left(\frac{\partial T}{\partial y}\right)_{y=0} + \left(q_r\right)_w \Rightarrow Nu = \frac{Nu_x}{\sqrt{\mathrm{Re}_x}} = -\left(1+\frac{4R}{3}\right)\theta'(0) \tag{18}$$

$$Sh_x = \left[-\left(\frac{x}{C_w - C_\infty}\right)\left(\frac{\partial C}{\partial y}\right)\right]_{y=0} \Rightarrow Sh = \frac{Sh}{\sqrt{\mathrm{Re}_x}} = -\left(\sqrt{\mathrm{Re}_x}\right)\phi'(0), \tag{19}$$

Where $\mathrm{Re}_x = \frac{ax}{\nu}$ is the local Reynolds number.

**Numerical Solutions by Runge-Kutta Shooting Technique:**

In the case of a full set of Eqs. (12)-(14), it seems that exact solutions are not possible. These results are the result of the nonlinear nature of (12)-(14), the requirement of numerical approaches to resolve the problem, and the inclusion of suitable boundary conditions in the formula (15). After being translated into a set of non-linear ordinary differential equations, which can be solved quantitatively via similarity transformations, the governing partial differential equations are solved numerically. It is necessary to combine the shooting methodology with a Runge-Kutta method in order to numerically solve the resulting boundary value issue. It is possible to get a collection of first-order differential equations by decomposing a set of nonlinear differential equations into a set of first-order differential equations. It has been demonstrated in the figure that the linked ordinary differential equations (12)-(14) may be reduced to a system of seven simultaneous equations for seven unknowns. The coupled ordinary differential Eqs. (12)-(14) are third order in $f(\eta)$ and second-order in $\theta(\eta)$ and $\phi(\eta)$ which have been reduced to a system of seven simultaneous equations for seven unknowns. In order to numerically solve this system of equations using Runge-Kutta method, the solutions require seven initial conditions but two initial conditions in $f(\eta)$ one initial condition in each of $\theta(\eta)$ and $\phi(\eta)$ are known. However, the values of $f'(\eta), \theta(\eta)$ and $\phi(\eta)$ are known at $\eta \to \infty$. These end conditions are utilized to produce unknown initial conditions at $\eta = 0$ by using shooting technique. The most important step of this scheme is to choose the appropriate finite value of $\eta_\infty$. Thus, to estimate the value of $\eta_\infty$ we start with some initial guess value and solve the boundary value problem consisting of Eqs. (12)-(14) to obtain $f''(0), \theta'(0)$ and $\phi'(0)$. The solution process is repeated with another larger value of $\eta_\infty$ until two successive values of $f''(0), \theta'(0)$ and $\phi'(0)$differ only after desired significant digit. The last value $\eta_\infty$ is taken as the finite value of the limit $\eta_\infty$ for the set of physical parameters for determining velocity, temperature, and concentration, respectively, are $f(\eta)$, $\theta(\eta)$ and $\phi(\eta)$in the boundary layer. After getting all the initial conditions we solve this system of simultaneous equations using fourth order Runge-Kutta integration scheme. Thus, the coupled boundary value problem of third-order in $f(\eta)$,second-order in $\theta(\eta)$ and $\phi(\eta)$ has been reduced to a system of seven simultaneous equations of first-order for seven unknowns as follows:

$$\left.\begin{aligned} & f' = p \Rightarrow f'' = p' = q \Rightarrow f''' = p'' = q' \\ & \Rightarrow q' = -fq + \left(\frac{2n}{n+1}\right)p^2 + Mp - \left(\frac{3(n-1)}{2}\right)We^2 q^2 fq' p^2 + Kp \\ & \theta' = r \Rightarrow \theta'' = r' \text{ then } r' = \frac{-(\mathrm{Pr})\, fr - (\mathrm{Pr})\, Nbrz - (\mathrm{Pr})(Nt)r^2}{\left(1+\frac{4R}{3}\right)} \\ & \& \ \phi' = z \Rightarrow \phi'' = z' \text{ then } z' = \frac{-(Le)(Nb)\, fz - 2(Nt)r'}{2Nb} \end{aligned}\right\} \tag{20}$$

and the corresponding boundary conditions became

$$f(0)=f_w,\ p(0)=1,\ \theta(0)=1,\ \phi(0)=1,\ p(\infty)\to 0,\ \theta(\infty)\to 0,\ \phi(\infty)\to 0$$

(21)

The boundary value problem is first converted into an initial value problem (IVP), which is then further explored. The beginning value problem is then solved by accurately guessing the missing starting value for various combinations of factors using the shooting method, which is repeated until the problem is solved. In this instance, the step size $h$ = 0.1 is used for calculating purposes. Additionally, a $10^{-6}$ error tolerance is being used. The information gathered is presented in the form of tables and graphs, with the main features of the problems addressed and explored in depth.

**Program Code Validation**

**Table-1.: Comparison of present $f'(\eta)$ profiles results with the published results of Rashidi et al. [25] at $We=M=K=R=0$**

| $\eta$ | Results of Rashidi et al. [25] | Present numerical results |
|---|---|---|
| 0.0 | 1.00000000 | 1.0000000000000000000 |
| 1.0 | 0.34838179 | 0.3470876157602564522 |
| 2.0 | 0.12812649 | 0.1365760764507265034 |
| 3.0 | 0.04815841 | 0.0354856862083756027 |
| 4.0 | 0.01825518 | 0.0170760766727560762 |
| 5.0 | 0.00694248 | 0.0056313242876806547 |
| 6.0 | 0.00264353 | 0.0014858723578206583 |

A very good validation of the present numerical results has been achieved with the numerical and analytical solutions results by Rashidi et al. [25] respectively as shown in table-1in absence of Carreau fluid, Porous medium, Thermal radiation, and Magnetic field.

## 4. Results and Discussion

In this research work, it is considered the radiative, steady Carreau-nanofluid flow of an incompressible, viscous, electrically conducting non-Newtonian fluid over a stretching sheet under the influence of magnetic field. The numerical solutions of the governing equations of the flow field are obtained by using RK – method along with shooting method. The flow is presided over by the non-dimensional parameters namely, Magnetic field parameter ($M$), Porous medium parameter ($K$), Suction/Injection parameter ($f_w$), Carreau fluid parameter ($We$), Stretching sheet parameter ($n$), Prandtl number (Pr), Thermal radiation parameter ($R$), Thermophoresis parameter ($Nt$), Brownian motion parameter ($Nb$) and Lewis number ($Le$).

- Fig. 2 depicts the influence of magnetic parameter on velocity profiles. It is observed that there is inverse relationship between magnetic parameter and velocity profiles. This is because with increase in magnetic parameter a force is produce, which is notable as Lorentz force. With the production of this force a resistive force induces, in opposite to the motion of fluid particles. Therefore, reduction takes place in profiles of velocity.
- Fig. 3 shows the effect of Carreau fluid parameter ($We$) on velocity profiles. Here we observe that the velocity profiles are decreasing function of Carreau fluid parameter.

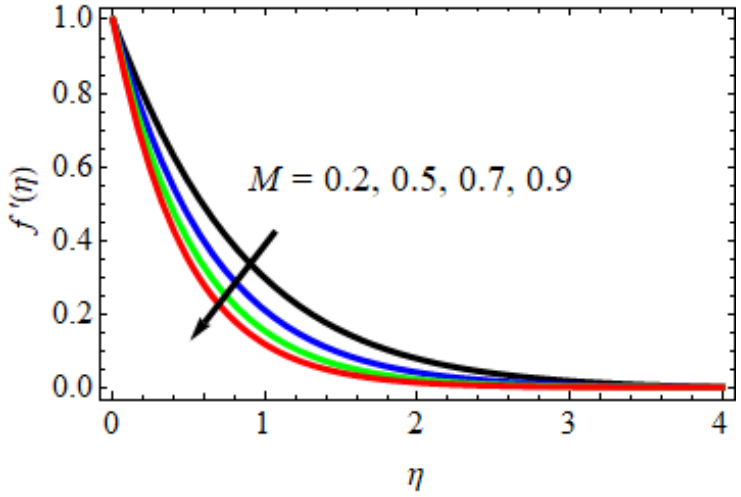


**Fig. 2.*M* effect on velocity profiles**

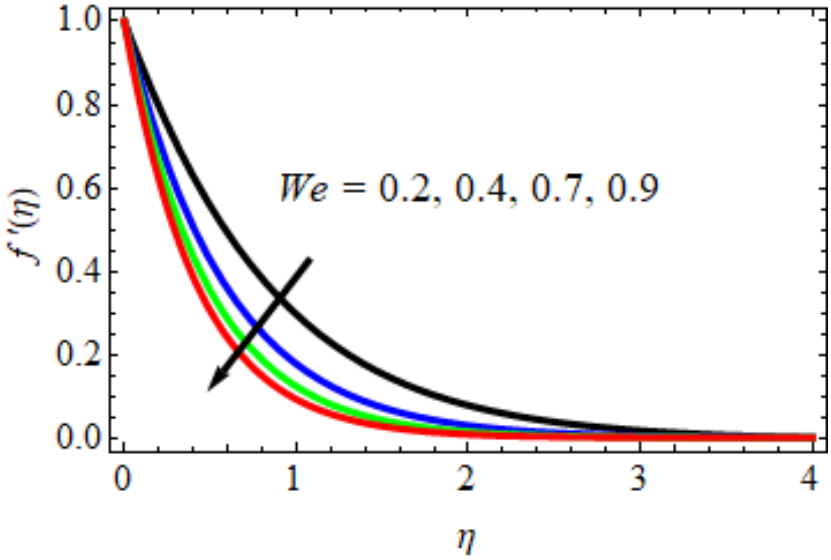


**Fig. 3. *We* effect on velocity profiles**

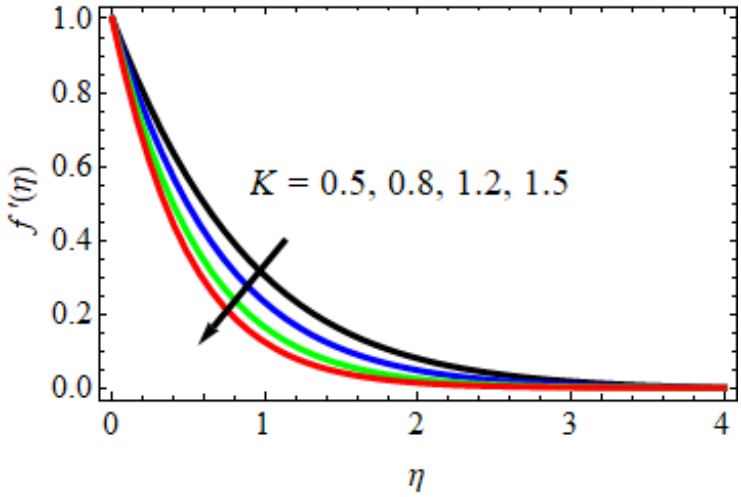


**Fig. 4. *K*effect on velocity profiles**

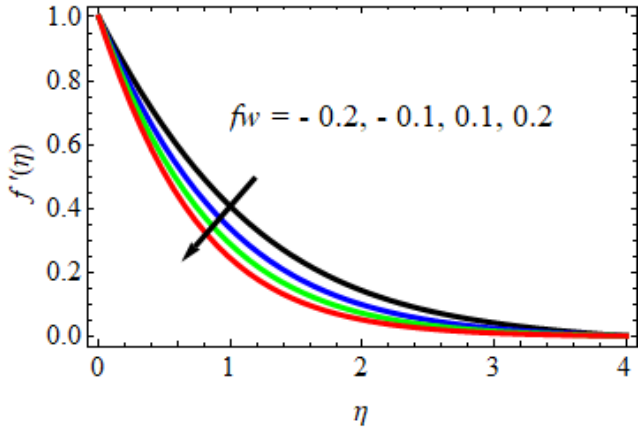


**Fig. 5.*fw* effect on velocity profiles**

➢ Fig. 4 illustrates the influence of the wall transpiration (i.e. suction/injection) parameter, $f_w$, on the evolution of velocity profiles in the stretching sheet boundary layer regime. The flow is observed to be strongly decelerated with suction ($f_w$ = 0.2) whereas it is accelerated markedly with increasing blowing (injection, $f_w$ = − 0.2). Suction causes the boundary layer to adhere more closely to the wall and this destroys momentum leading to a plummet in velocity. Momentum boundary layer thickness is therefore decreased with suction. Conversely injection adds nanofluid via lateral mass flux through the sheet and this assists momentum development, enhancing velocity and causing a concomitant increase in momentum boundary layer thickness.It is interesting to note that suction does not, however induce flow reversal-velocity remains positive throughout the boundary layer regime. Excellent flow control is therefore achieved in the nanofluid sheet regime with suction.

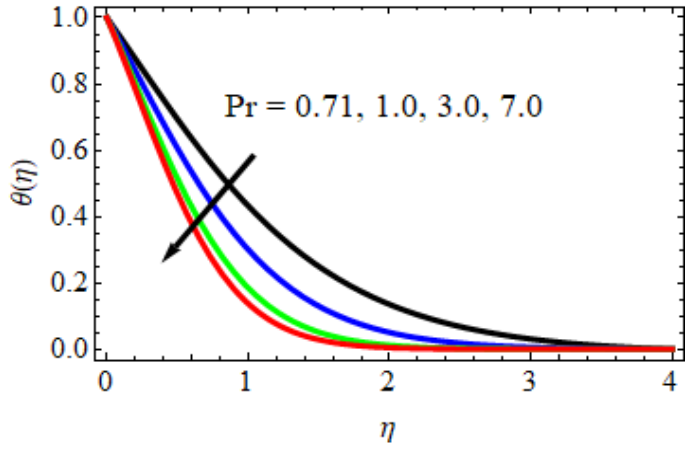


**Fig. 6.Pr effect on temperature profiles**

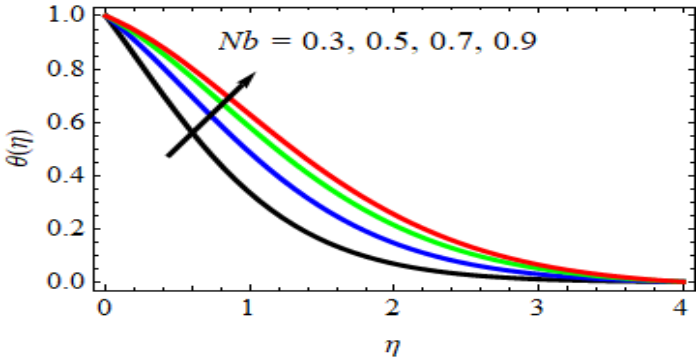


**Fig. 7.*Nb* effect on temperature profiles**

➢ Fig. 5 illustrates the effect of Permeability parameter (*K*) on the velocity distribution. From this figure, it is observed that the velocity profile decreases with the increased in the Permeability (porosity) parameter *K*. This arises due to the fact that an increase in *K* amplifies the porous layer and thereby reduces the thickness of momentum boundary layer.

➢ Fig. 6 presents the effect of Prandtl number (Pr) on the fluid temperature. As the value of Pr increases, the temperature gradient of the fluid decreases. As Pr increases, the momentum diffusivity increases and dominates the thermal diffusivity. The fluid velocity is high enough to help the heat transfer of the fluid. This makes the heat dissipation rate faster and makes the boundary layer to become thinner.

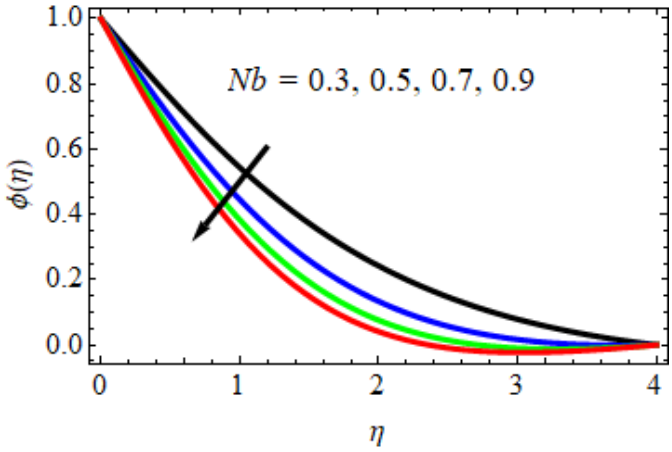


**Fig. 8.*Nb* effect on concentration profiles**

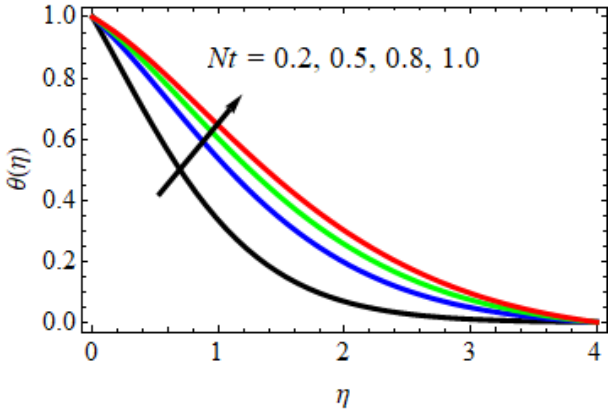


**Fig. 9.*Nt* effect on temperature profiles**

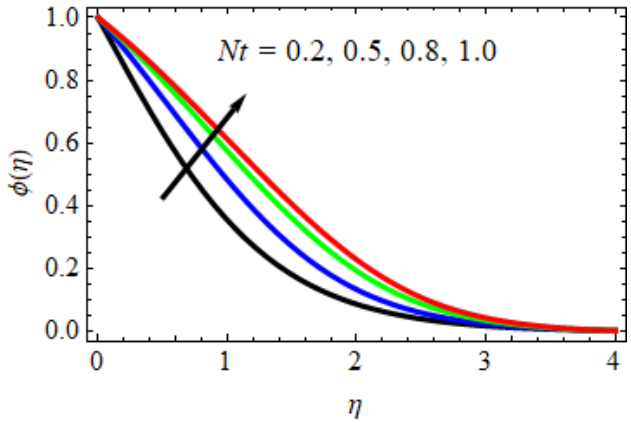


**Fig. 10.*Nt* effect on concentration profiles**

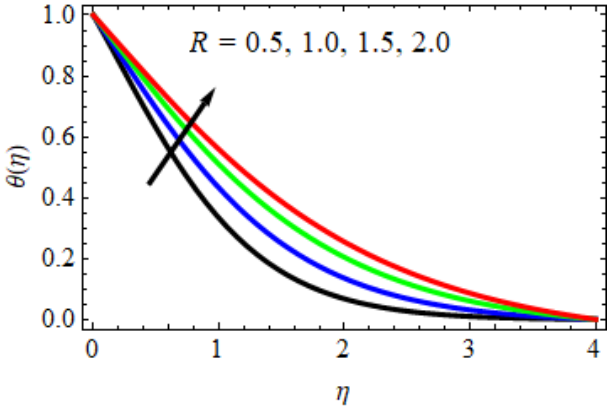


**Fig. 11.*R* effect on temperature profiles**

➢ The Brownian movement parameter (*Nb*) then, at that point the Thermophoresis limitation (*Nt*) affect the dimensionless temperature & nanoparticle concentration profiles, as exposed in Figs. 7 to 10. The temperature profile appears to increase as the Brownian motion parameter (*Nb*) is increased, while the nanoparticle volume concentration profile drops. We also find that as the Thermophoresis parameter (*Nt*) is increased, the dimensionless temperature & nanoparticle volume portion rise. This remains because the temperature gradient produces the Thermophoretic force, which causes an extremely high-speed flow away from the stretching sheet. As the Thermophoresis parameter (*Nt*) develops, the liquid is warmed and moves from the extending surface, and thus, the warm limit layer width increments, also the temperature slope at the surface reductions as both *Nt*&*Nb* esteem increment.

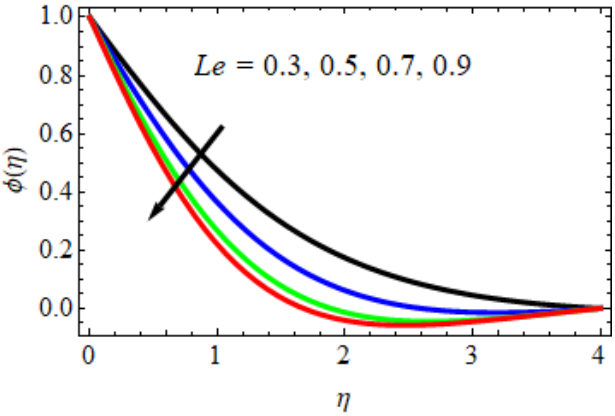


**Fig. 12.*Le* effect on concentration profiles**

➢ Fig. 11 shows that the thermal radiation parameter (*R*) has an influence on the temperature distribution $\theta(\eta)$. Heat dispersion increases when the thermal radiation parameter *R* is raised over its default value. As the value of *R* is raised, the thermal buoyancy force increases and the thickness of the thermal boundary layer decreases. On a physical level, increasing the thermal radiation parameter *R* causes more heat to be created in the fluid flow zone, resulting in more uniform temperature distributions $\theta(\eta)$.

➢ Fig. 12 depicts the influence of the Lewis number (*Le*) on concentration profiles. The dimensionless Lewis number is defined as the ratio of thermal and mass diffusivity. It is noticed that the nano particle volume fraction experiences a strong reduction for the values of *Le*.

➢ Table-2 shows the numerical values of Skin-friction coefficient (*Cf*) for variations in values of the engineering parameters such as, *M*, $f_w$, *We*, *n*, *K*, Pr, *R*, *Nb*, *Nt* and *Le*. From this table, it is observed that the

Skin-friction coefficient is increasing with rising values of *Nb*, *R* and *Nt*, while it is decreasing with increasing values of *We*, *M*, $f_w$, *n*, *K*, Pr, and *Le*.

➢ The numerical values of rate of heat transfer coefficient in terms of Nusselt number ( $Nu_x$ ) are displayed in Table-3 for different values of Pr, *Nb*, *Nt* and *R*.The rate of heat transfer coefficient is gradually rising with increasing values of *R*, *Nb* and *Nt*, while the reverse effect is observed in increasing values of Pr.

➢ The effects of *Nb*, *Nt*and *Le* on rate of mass transfer coefficient or in terms of Sherwood number coefficient ( $Sh_x$ ) are discussed in Table-4. From this table, it is observed that the reduced rate of mass transfer coefficient is increasing with increasing values of *Nt* and decreasing with increasing values of *Nb* and *Le*.

**Table-2.: Numerical values of skin-friction coefficient (*Cf*) for variations of *M*, $f_w$, *We*, *n*, *K*, Pr, *R*, *Nb*, *Nt* and *Le***

| *M* | $f_w$ | *We* | *n* | *K* | Pr | *R* | *Nb* | *Nt* | *Le* | *Cf* |
|---|---|---|---|---|---|---|---|---|---|---|
| 0.2 | - 0.2 | 0.2 | 0.1 | 0.5 | 0.71 | 0.5 | 0.3 | 0.2 | 0.3 | 1.4575256027239 |
| **0.5** | | | | | | | | | | 1.4187687812872 |
| **0.7** | | | | | | | | | | 1.3976582182468 |
| | **- 0.1** | | | | | | | | | 1.4265876192856 |
| | **0.1** | | | | | | | | | 1.3958768765891 |
| | **0.2** | | | | | | | | | 1.3766087609876 |
| | | **0.4** | | | | | | | | 1.4356868165898 |
| | | **0.7** | | | | | | | | 1.4065659641291 |
| | | | **0.3** | | | | | | | 1.4189682425452 |
| | | | **0.5** | | | | | | | 1.3856896987634 |
| | | | | **0.8** | | | | | | 1.4156587672342 |
| | | | | **1.2** | | | | | | 1.3790668678688 |
| | | | | | **1.00** | | | | | 1.4065876876134 |
| | | | | | **3.00** | | | | | 1.3687687656181 |
| | | | | | | **1.0** | | | | 1.4965876180568 |
| | | | | | | **1.5** | | | | 1.5214255982897 |
| | | | | | | | **0.5** | | | 1.4858598289154 |
| | | | | | | | **0.7** | | | 1.5051859825982 |
| | | | | | | | | **0.5** | | 1.5076475217346 |
| | | | | | | | | **0.8** | | 1.5258769876125 |
| | | | | | | | | | **0.5** | 1.4159956345859 |
| | | | | | | | | | **0.7** | 1.3908676062361 |

**Table-3.: Numerical values of reduced rate of heat transfer coefficient ( $Nu_x$ ) for different values of Pr, *Nb*, *Nt*and *R***

| Pr | *Nb* | *Nt* | *R* | $Nu_x$ |
|---|---|---|---|---|
| 0.71 | 0.5 | 0.5 | 0.5 | 0.561548548259828 |
| **1.00** | | | | 0.514589258925367 |
| **3.00** | | | | 0.497856523547625 |
| | **0.8** | | | 0.597634652745922 |
| | **1.0** | | | 0.613576185782436 |
| | | **0.8** | | 0.584664554726872 |
| | | **1.0** | | 0.601582589256822 |
| | | | **0.8** | 0.539876876452568 |
| | | | **1.0** | 0.516787987325676 |

**Table-4.: Numerical values of rate of mass transfer coefficient ( $Sh_x$ ) for various values of *Nb*, *Nt* and *Le***

| *Nb* | *Nt* | *Le* | $Sh_x$ |
|---|---|---|---|
| 0.5 | 0.5 | 0.5 | 0.664572345722962 |
| **0.8** | | | 0.630988979898238 |
| **1.0** | | | 0.615485982586145 |
| | **0.8** | | 0.685656868612585 |
| | **1.0** | | 0.704765471256971 |
| | | **1.0** | 0.645659659123415 |
| | | **1.2** | 0.617687653134576 |

## 5. Conclusions

This report presents a numerical investigation of steady-magnetohydrodynamic Carreau-nanofluid, highlighting the derivation of non-linear ordinary differential equations governing velocity, concentration, and temperature profiles in the presence of magnetic field, thermal radiation, porous medium towards a non-linear stretching sheet with transpiration effects. By employing the Runge-Kutta method along with shooting technique and visual aids such as graphs and tables, the study verifies convergence and offers valuable insights for developing efficient fluid systems at the nanoscale. It is worth concluding that.

➢ A rise in the Carreau fluid parameter amplifies the non-Newtonian effects, which in turn leads to an increase in the viscosity of the fluid and has an impact on the internal velocity profiles, which are essential for the precise regulation of flow. By gaining an understanding of its effect, one may make the process of designing and studying systems that include non-Newtonian fluids easier, which ultimately leads to improvements in both efficiency and performance.

➢ Regarding fluids with high conductivity, the strength of the magnetic field greatly affects the velocity profiles, leading to the emergence of resistive forces that alter the flow patterns. The Lorentz force acts as a resistive force, reducing the velocity of the fluid, due to the influence of the magnetic field parameter *M*. Due to this phenomenon, there are observable flow patterns that affect the distribution of velocity. This phenomenon is especially noticeable in fluids with high conductivity when they are exposed to strong magnetic fields.

➢ The intricate relationship between the volume fraction of nano particles and the velocity of fluids emphasizes the need of meticulous thought while performing experiments on nano fluids. By augmenting the proportions of nano particles in the fluid, it is feasible to modify the fluid's viscosity, thereby impacting the flow dynamics and perhaps leading to non-Newtonian behaviour.

➢ In program code validation, the obtained results are in good agreement with the published results of Rashidi et al. [25] at $We = M = K = R = 0$.

**Nomenclature:**

**List of Symbols:**

$u, v$ : Velocity components in $x$ and $y$ axes respectively ($m/s$)

$x, y$ : Cartesian coordinates measured along the stretching sheet ($m$)

$f$ : Dimensionless stream function

$f'$ : Fluid velocity ($m/s$)

Pr : Prandtl number

$C$ : Fluid concentration $\left(mol/m^3\right)$

$C_\infty$ : Dimensional ambient volume fraction $\left(mol/m^3\right)$

$T$ : Fluid temperature $\left(K\right)$

$T_w$ : Temperature at the surface $\left(K\right)$

$Cf$ : Skin-friction coefficient

$T_\infty$ : Temperature of the fluid far away from the stretching sheet $\left(K\right)$

$M$ : Magnetic field parameter

$C_w$ : Dimensional concentration at the stretching surface $\left(mol/m^3\right)$

$Nu_x$ : Rate of heat transfer coefficient (or) Nusselt number

$Sh_x$ : Rate of mass transfer coefficient (or) Sherwood number

$C_f$ : Specific heat capacity at constant pressure

$C_p$ : Specific heat capacity of nanoparticle material

$B_o$ : Uniform magnetic field

$Le$ : Lewis number

$U$ : Reference velocity $\left(m/s\right)$

$Nb$ : Brownian Motion parameter

$Nt$ : Thermophoresis parameter

$D_B$ : Brownian diffusion coefficient

$D_T$ : Thermophoresis diffusion coefficient

$a$ : Positive real number

$u_w$ : Stretching velocity of the fluid along $x$ - direction($m/s$)

$v_w$ : Stretching velocity of the fluid along $y$ - direction($m/s$)

$q_r$ : Radiative heat flux

$g$ : Acceleration due to gravity($m/s^2$)

$R$ : Thermal radiation parameter

$K^*$ : Mean absorption coefficient

$n$ : Non-linear stretching parameter

$O$ : Origin

$K_o$: Dimensional Permeability parameter

$K$ : Non-dimensional Permeability Parameter

$Nu$ : Rate of heat transfer coefficient (or) Nusselt number

$Sh$ : Rate of mass transfer coefficient (or) Sherwood number

$We$ : Carreau fluid parameter

$fw$ : Suction/Injection parameter

$q_w$: Heat flux

$q_m$: Mass flux

**Greek symbols:**

$\eta$ : Dimensionless similarity variable

$\theta$ : Dimensionless temperature $(K)$

$\alpha_m$ : Nanofluid thermal diffusivity $(m^2/s)$

$\nu$ : Kinematic viscosity $(m^2/s)$

$\phi$ : Dimensionlessnanofluid concentration $(mol/m^3)$

$\sigma^*$ : Stefan-Boltzmannconstant

$\rho_p$ : Density of nanoparticle material

$\sigma$ : Electrical Conductivity

$\rho$ : Fluid density ($kg/m^3$)

$\rho_f$ : Density of the fluid($kg/m^3$)

$\tau$ : Cauchy Stress tensor

**Superscript:**

$'$ : Differentiation w.r.t $\eta$

**Subscripts:**

$f$ : Fluid

$w$ : Condition on the sheet

$\infty$ : Ambient Conditions

**References**

[1] Carreau Pierre J., Rheological equations from molecular network theories,Trans. Soc. Rheol., 16 (1) (1972), pp. 99-127.

[2] M. Farooq, M. I. Khan, M. Waqas, T. Hayat, A. Alsaedi, M. I. Khan, MHD Stagnation point flow of viscoelastic nanofluid with non-linear radiation effects, J. Mol. Liq., 221 (2016), pp. 1097-1103.

[3] C. Sulochana, G. P. Ashwinkumar, N. Sandeep, Transpiration effect on stagnation-point flow a Carreau nanofluid in the presence of thermophoresis and Brownian motion, Alex. Eng. J., 55 (2016), pp. 1151-1157.

[4] M. Khan, Md. Azam, A. S. Alshomrani, On unsteady heat and mass transfer in Carreau nanofluid flow over expanding or contracting cylinder with convective surface conditions, Journal of Molecular Liquids, Vol. 231, 2017, pp. 474-484.

[5] M. Khan, M. Azam, Unsteady heat and mass transfer mechanisms in MHD Carreau nanofluid flow, J. Mol. Liq., 225 (2017), pp. 554-562.

[6] M. Khan, M. Azam, A. Munir, On unsteady Falkner-Skan flow of MHD Carreau nanofluid past a static/moving wedge with convective surface condition, J. Mol. Liq., 230 (2017), pp. 48-58.

[7] C. S. K. Raju, N. Sandeep, Falkner-Skan flow of magnetic-Carreau fluid past a wedge in the presence of cross diffusion effects, Eur. Phys. J. Plus, 131 (2016), p. 267.

[8] M. I. Khan, T. Hayat, S. Afzal, M. I. Khan, A. Alsaedi, Theoretical and numerical investigation of Carreau-Yasuda fluid flow subject to Soret and Dufour effects, Comput. Methods Programs Biomed., 186 (2020), Article 105145.

[9] H. Waqas, S. U. Khan, M. M. Bhatti, M. Imran, Significance of bioconvection in chemical reactive flow of magnetized Carreau–Yasuda nanofluid with thermal radiation and second-order slip, J. Therm. Anal. Calorim., 140 (2020), pp. 1293-1306.

[10] Riaz A., Abbas T., ul Ain A. Q., Nanoparticles phenomenon for the thermal management of wavy flow of a Carreau fluid through a three-dimensional channel, J. Therm. Anal. Calorim., 143 (3) (2021), pp. 2395-2410.

[11] Hayat T., Asad S., Mustafa M., Alsaedi A., Boundary layer flow of Carreau fluid over a convectively heated stretching sheet, Appl. Math. Comput., 246 (2014), pp. 12-22.

[12] Waqas M., Khan M. I., Hayat T., Alsaedi A., Numerical simulation for magneto Carreau nanofluid model with thermal radiation: A revised model, Comput. Methods Appl. Mech. Engrg., 324 (2017), pp. 640-653.

[13] Irfan M., Rafiq K., Khan W. A., Khan M., Numerical analysis of unsteady Carreau nanofluid flow with variable conductivity, Appl. Nanosci., 10 (2020), pp. 3075-3084.

[14] Irfan M., Khan M., Khan W. A., Physical aspects of shear thinning/thickening behaviour in radiative flow of magnetite Carreau nanofluid with nanoparticle mass flux conditions, Appl. Nanosci., 10 (2020), pp. 3021-3033.
[15] Irfan M., Study of Brownian motion and thermophoretic diffusion on non-linear mixed convection flow of Carreau nanofluid subject to variables properties, Surf. Interfaces, 23 (2021), Article 100926.
[16] Tanmay V. S., Stability of plane Couette flow of Carreau fluid past a deformable solid at arbitrary Reynolds number, Results Phys., 30 (7) (2018).
[17] Khan M., Azam M., Alshomrani A. S., Unsteady slip flow of Carreau nanofluid over a wedge with nonlinear radiation and new mass flux condition, Results Phys., 7 (2017), pp. 2261-2270.
[18] Khan M., Azam M., Alshomrani A. S., Effects of melting and heat generation/absorption on unsteady Falkner-Skan flow of Carreau nanofluid over a wedge, Int. J. Heat Mass Transfer, 110 (2017), pp. 437-446
[19] T. Hayat, N. Saleem, N. Ali, Effect of induced magnetic field on peristaltic transport of a Carreau fluid, Commun. Nonlinear Sci. Numer. Simul., 15 (9) (2010), pp. 2407-2423.
[20] K. U. Rehman, W. Shatanawi, K. Abodayeh, A group theoretic analysis on heat transfer in MHD thermally slip Carreau fluid subject to multiple flow regimes (MFRs), Case Stud. Therm. Eng., 30 (2022), Article 101787.
[21] T. Salahuddin, M. Awais, A comparative study of Cross and Carreau fluid models having variable fluid characteristics, Int. Commun. Heat Mass Transfer, 139 (2022), Article 106431.
[22] Tanveer A., Hayat T., Alsaedi A., Ahmad B., Numerical simulation for peristalsis of Carreau-Yasuda nanofluid in curved channel with mixed convection and porous space, PLoS One, 12 (2) (2017), Article e0170029
[23] Abdollahzadeh Jamalabadi M. Y., Daqiqshirazi M., Nasiri H., Safaei M. R., Nguyen T. K., Modeling and analysis of biomagnetic blood Carreau fluid flow through a stenosis artery with magnetic heat transfer: A transient study, PLoS One, 13 (2) (2018), Article.
[24] P. Rana, R. Bhargava (2012), Flow and heat transfer of a nanofluid over a nonlinearly stretching sheet: a numerical study. Commun. Nonlinear Sci. Numer. Simul., 17, pp. 212-226.
[25] M. M. Rashidi, N. Freidoonimehr, A. Hosseini, O. Anwar Bég, T.-K. Hung, (2014). Homotopy simulation of nanofluid dynamics from a non-linearly stretching isothermal permeable sheet with transpiration, Meccanica,Vol. 49, pp. 469-482.
[26] G Murali, A Paul, NVN Babu, Heat and mass transfer effects on an unsteady hydromagnetic free convective flow over an infinite vertical plate embedded in a porous medium with heat absorption, *Int. J. Open Problems Compt. Math* 8 (1), 2015.
[27] Deepa Gadipally,Murali Gundagani,Analysis of soret and dufour effects on unsteady MHD flow past a semi infinite vertical porous plate via finite difference method, *International journal of applied physics and mathematics*,4(5),332-344,2014. **DOI:** 10.7763/IJAPM.2014.V4.306.
[28] NVN Babu, Ajit Paul,G Murali, Soret and Dufour effects on unsteady hydromagnetic free convective fluid flow past an infinite vertical porous plate in the presence of chemical reaction, *Journal of science and arts*, 15 (1), pp. 99-111, 2015.
[29] Murali Gundagani, MCK Reddy,Sivaiah (2012) Finite element solution of thermal radiation effect on unsteady MHD flow past a vertical porous plate with variable suction *American Academic & Scholarly Research Journal* 4 (3), 3-22,2012.
[30] Babu, N.V.N.,Murali, G., Bhati, S.M.(2018). Casson fluid performance on natural convective dissipative couette flow past an infinite vertically inclined plate filled in porous medium with heat transfer, MHD and hall current effects, *International journal of Pharmaceutical Research, 10*(4), 2018.
[31] G. Murali1 , G. Deepa, Nirmala Kasturi V , T. Poornakantha (2023),Joint effects of thermal diffusion and diffusion thermo on MHD three dimensional nanofluid flow towards a stretching sheet, *Mathematical models in engineering*, DOI https://doi.org/10.21595/mme.2023.23590.
[32] Gundagani, M., Babu, N.V.N., Gadially, D. *et al.* Study of Nano-Powell-Erying fluid flow past a porous stretching sheet by the effects of MHD, thermal and mass convective boundary conditions. *J. Umm Al-Qura Univ. Eng. Archit.* (2024). https://doi.org/10.1007/s43995-024-00056-2

[33] Gundagani, M., Mamidi, L.P. & Tanuku, P.K. Finite element solutions of Double diffusion effects on three-dimensional MHD Nano-Powell-Erying fluid flow in presence of thermal and mass Biot numbers. *J. Eng. Appl. Sci.* 71, 9 (2024). https://doi.org/10.1186/s44147-023-00347-w

[34] Murali G, NVN Babu, Convective MHD Jeffrey Fluid Flow Due to Vertical Plates with Pulsed Fluid Suction:A Numerical Study, *Journal of computational applied mechanics* DOI *10.22059/JCAMECH.2023.351326.773,2023.*